NASE

Natural Sciences and Engineering Bulletin

May 2025, 2(1)
Received: 17/01/2025
Accepted: 02/05/2025

RESEARCH ARTICLE http://dergipark.gov.tr/nase

Performance Evaluation of Flywheel, Battery and Superconducting Magnetic Energy Storage Systems on Frequency Regulation in the Context of Renewable Energy Integration

Ahmet Mete Vural[1*], Aliyu Garba Ibrahim[2]

Keywords
Battery energy storage,
Flywheel energy storage,
Superconducting energy storage,
Wind turbine,
Photovoltaic,
Artificial rabbit optimization,
Lightning search algorithm,
Whale optimization algorithm

Abstract – Frequency regulation is a crucial aspect of power system operation as it ensures that the power systems operate in a stable manner. Variations in load and renewable energy generation are the main causes of frequency instability due to weather uncertainty. This paper investigates the effects of variations in load and renewable energy generation on frequency control in power systems. Also, three different energy storage technologies (Flywheel, Battery, and Superconducting Magnetic Energy Storage) are integrated to test systems to investigate their effects on frequency control. To enhance the dynamic performance of the frequency controller, three recent optimization methods (Artificial Rabbit Optimization, Lightning Search Algorithm, and Whale Optimization Algorithm) are utilized when the test systems are subjected to different operating conditions and disturbances. The superiority of the Artificial Rabbit Optimization in comparison with other optimization methods is shown in effectively mitigating frequency oscillations in both single-area and two-area test systems. The energy storage solutions are evaluated in terms of damping effect, transient stability, and integral time absolute error index in two test systems. A compressive simulation study is conducted, and the results are presented and discussed.

1. Introduction

The world has seen a massive investment in renewable energy research and invention due to the living reality of global warming disasters such as acid rain, the recent wildest forest fire-like inferno, and drought. Renewable energy source (RES) is the only option out of this disaster and at the backbone of the RES. Energy storage system (ESS) stands to smoothen the integration and prevent power outages. Integrating ESSs and power-reserved synchronization is an effective solution for overcoming RES intermittency and fluctuating effects. On the other hand, frequency regulation is a key component of maintaining stability and reliability in electrical power systems. This process ensures that the system frequency remains within designated limits despite fluctuations in power demand and supply. These fluctuations are primarily caused by changes in consumer load and the unpredictable nature of RES, like wind and solar power. Advanced control strategies and optimization algorithms are necessary to mitigate frequency deviations when the power systems are faced with various disturbances such as sudden load variation, fault, and unpredictable RES generation. ESS provides frequency regulation by dynamically injecting/absorbing power to/from the grid in response to a decrease/increase in frequency. Due to fast response time, ESS technology can inject large amounts of power into the grid in the shortest period, which can be used as virtual inertia. The two most important aspects related to applying fast responsive energy storage technologies for frequency regulation services that, control and sizing, are discussed

[1*]**Corresponding Author.** Electrical and Electronics Engineering Department, Gaziantep University, 27310 Gaziantep, Türkiye.
E-mail: mvural@gantep.edu.tr OrcID: 0000-0003-2543-4019
[2] Graduate School of Applied and Natural Sciences, Gaziantep University, 27310 Gaziantep, Türkiye.
E-mail: aliyu.gibrahim@yahoo.com OrcID: 0009-0000-4499-4324
Citation: Vural, A. M. and Ibrahim, A. G. (2025). Comparison of flywheel, battery and superconducting magnetic energy storage systems for frequency regulation. *Natural Sciences and Engineering Bulletin, 2*(1), 26-55.

in detail for both single and hybrid storage technologies (Akram et al, 2020). In the literature, frequency regulation studies are multifaceted in terms of the type of RES used, the type of controller, and the kind of system disturbance. An adaptive control strategy to coordinate the generator and the governor with an ESS in frequency regulation has been proposed (Ibrahim et al., 2022). The comparison between the ESS compensation with a conventional droop control and the proposed method has been used. The simulation results show that compared to the ESS with a fixed droop control scheme; and the proposed control scheme provides better results in regulating the frequency response by lowering the rate of change of frequency and improving the minimum frequency deviations during the generator tripping events. The droop control is not generally able to generate a large power output immediately after the disturbance, while it increases the power output with the increment of frequency deviation. In another research, superconducting magnetic energy storage system (SMESS) and battery energy storage system (BESS) based hybrid energy storage systems are designed to reduce grid voltage fluctuations, and a new ever-triggered control system is proposed for SMESS to improve the microgrid's voltage and frequency stability (Vishnuvardhan and Saravanan, 2023). The multimachine system stability analysis of interconnected 375 MW hybrid wind and solar photovoltaic (PV) systems is connected with SMESS energy storage. Analyzing the performance metrics of BESSs at different levels of penetrations of RES has been addressed (Li et al., 2023). By quantitatively evaluating the impact of BESSs with various energy-to-power ratios, it has been deduced that as the penetration of RES increases, the storage systems with higher energy-to-power ratio are favored. The effectiveness of BESS in providing primary frequency control has been addressed when applied to a weak grid system (Julius et al., 2022). The state of charge (SOC) restoration logic has been considered to ensure service continuity and effective frequency regulation. The optimal size of BESS installation to accomplish the goal has also been studied with a dynamic grid model. Research and inventions have been overflowing in the conventional proportional integral (PI) and proportional integral derivative (PID) types of controllers and their parameter optimization in power systems. The PID controller is tuned using different optimization methods with comparison and a novel genetic algorithm-fuzzy logic self-tuning technique is suggested (Ali et al., 2024). Results show the suggested method outperforms others in restoring power system stability. The artificial rabbit optimization (ARO) method is used to tune the controller parameters in a microgrid, ensuring stability under major disturbances (Khalil et al., 2023). Sensitivity analysis with +-25% parameter variations confirms the robustness of the approach. The study suggests a bat-inspired optimization algorithm which is modeled on animal echolocation behavior (Ramesh Kumar et al., 2013). This optimization approach is used to enhance load frequency control (LFC) in a two-area power system with SMESS unit. Elsisi et al., (2018), introduces the Gravitational Search Algorithm and Bat-inspired Algorithm as two techniques for designing model predictive controller for LFC. The power system is embedded with SMESS and compressive energy storage. The study of Ray et al., (2019), proposes a hybrid firefly particle swarm optimization (PSO) technique to tune PID controller parameters for minimizing frequency deviation in a microgrid under varying wind speeds and load demands. Comparative analysis with PSO and firefly algorithms have been carried out using various performance indices. The integration of RES into power grids presents significant challenges, particularly in maintaining frequency stability due to their intermittent nature. Extensive research has been conducted on frequency control strategies for single renewable energy integration with standalone energy storage systems (Wang et al., 2022a; Yao et al., 2016) modeling ESS for grid (Hutchinson et al., 2024; Cansiz et al., 2017; Georgious et al., 2021; Hajiaghasi et al., 2019; Lin and Zamora, 2022; Peralta et al., 2018; Qu and Ye, 2023; Santhi et al., 2013; Worku, 2022) frequency regulation, and the economic comparison of different ESS technologies (Mcllwaine et al., 2021; Moradi-Shahrbabak and Jadidoleslam, 2023; Ranjan Chakraborty et al., 2022; Rouniyar and Karki, 2021; Sassi et al., 2017). Additionally, studies have explored coordinated control strategies for hybrid storage systems (Nguyen-Huu et al., 2020), optimization-based enhancements for conventional controllers (Sahu et al., 2015), and the role of ESS in mitigating frequency fluctuations caused by hybrid RES penetration (Ibraheem et al., 2022; Mugyema et al., 2023). However, these studies often focus on isolated aspects of the problem rather than providing a comprehensive solution. This paper bridges these research gaps by integrating all these critical aspects into a unified framework. By combining modeling, economic considerations, control strategies, and optimization techniques with extensive simulation cases, this study presents a holistic approach to frequency regulation, offering a more robust and practical solution for modern power grids facing increasing renewable energy penetration.

The main contributions of this paper are:

1. LFC of single-area and two-area systems to achieve a high level of stability and robustness due to the penetration of RES such as PV and wind turbine (WT) is realized.
2. The contribution of FESS, BESS, and SMESS in the LFC is evaluated by comparison.
3. The comparison of optimization methods such as ARO, LSA, and WOA in enhancing the controller parameters for effective mitigation of frequency instability during severe disturbances is carried out.

The paper is structured as follows: After the introductory section, Section 2 presents the modeling of a single-area power system, the relevant parts, and their transfer functions. The introduction of the RES, such as PV and WT, and the role they play in the system in a different weather condition and their transfer function. A dedicated subsection will provide detailed information about the ARO algorithm, the leading algorithm in this work, for better optimization and enhancing the PID parameter. The third subsection is for results and discussion of the simulations, which presents the simulation results obtained from both test systems under different operating scenarios. The detailed discussion is also made on the obtained results. The PID parameter tuning performances of ARO, lighting search algorithm (LSA), and whale optimization algorithm (WOA) methods are evaluated in detail, together with the effects of various ESSs in the frequency control operation under optimized parameters of ARO. The general conclusions are drawn at the end.

2. Materials and Methods

2.1. Modeling of the single-area system

The transfer function model of the single-area power system is illustrated in Figure 1. The generator inertia constant is defined by H=5. The turbine acts as the mechanical power source with its dynamics defined by a time constant T_t=0.5s. The governor with the time constant, T_g=0.2 s detects speed changes and modulates the turbine input to restore the steady-state operation. The governor's typical speed regulation is defined as R=20, the percentage change of speed from no-load to full-load. The inertia load, incorporating both rotating masses and the connected load is quantified by the proportionality constant D=0.8, which represents the percentage change in load per percentage change in frequency (Ray et al., 2019).

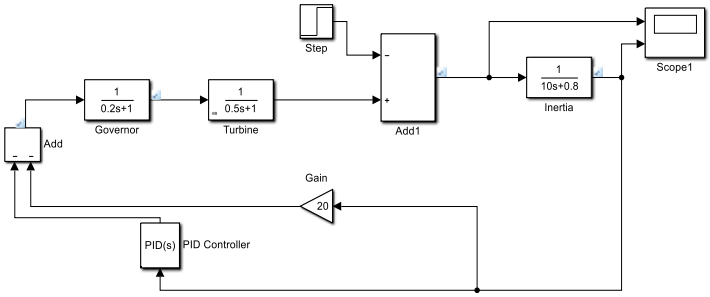

Figure 1. Transfer function representation of the single-area power system

2.2. Modeling of the two-area system

The two-area power system is usually modelled as two separate generation locations, each of which is modelled using an ideal AC voltage source and a reactance connected in series. Then, the outputs of these locations are connected with a tie line. By this way, the steady-state behavior of this system can be modelled in its simplest form. The tie-line active power flow from area-1 to area-2 when neglecting losses can be calculated,

$$P_{12} = \frac{|E_1||E_2|}{X_{12}} \, sin\varphi_{12} \tag{1}$$

where, E_1 and E_2 respectively represent the output voltage of each generator, X_{12} is the tie-line reactance, and φ_{12} is the phase angle difference between each generator output. The tie line power deviation is represented by (2), which is perceived as an increase in load in one area and a corresponding decrease in the other, depending on the flow's direction. This direction is determined by the difference in phase angle between the two areas. For instance, if $\Delta\varphi_1 - \varphi$ is positive, the active power flows from area 1 to 2. P_s is the synchronizing power

coefficient. The conventional LFC relies on tie-line bias control as shown in (3), where each control area aims to minimize the area control error (ACE) to zero. The ACE in each area is a combination of frequency deviation and tie-line power flow error.

$$\Delta P_{12} = P_s(\Delta\varphi_1 - \Delta\varphi_2) \tag{2}$$

$$ACE_i = \sum_{j=1}^{n} \Delta p_{ij} + k_i \Delta f \tag{3}$$

The area bias k_i determines the level of interaction between neighboring areas during a disturbance. Optimal performance is achieved when k_i is set to the frequency bias factor of that area, $B_i = \beta_i + D_i$. For a two-area system, the ACE equations are given as,

$$ACE_1 = \Delta P_{12} + B_1 \Delta F_1 \tag{4}$$

$$ACE_2 = \Delta P_{21} + B_2 \Delta F_2 \tag{5}$$

B_1 and B_2 are known as frequency bias factors, ΔP_{12} and ΔP_{12} are changes in power output in both areas. Each area is modeled with an equivalent turbine and governor, and the incremental power balance is controlled by the tie-line bias control which is the ACE. In this study, the parameters of the two-area system are listed in Table 1 (Saadat, 1999). The synchronizing power coefficient P_s is taken as 2.0 p.u. The transfer function representation of the two-area power system is depicted in Figure 2.

Table 1. Parameters of the two-area power system

Parameter Name	Area-1	Area-2
Speed Regulation (R)	0.05	0.0625
Frequency Load Coefficient (D)	0.6	0.9
Inertia constant (H)	5	4
Base power(s)	1000MVA	1000MVA
Governor Time Constant ($\boldsymbol{T_g}$)	0.2	0.3
Turbine Constant ($\boldsymbol{T_t}$)	0.5	0.6
Integrator gain ($\boldsymbol{K_i}$)	0.3	0.3
Nominal frequency	60Hz	60Hz

2.3. PV and WT models

The PV model can be expressed as the product of three transfer functions as given in (6) (Ibraheem et al., 2022). This model provides sufficient small signal behavior to capture the power dynamics of the PV system. The parameters are T_{pv}=1.8, which indicates the speed response of the PV system, T_{in}=0.04, which is the time constant that represents how quickly the inverter dynamics react to changes from the PV system, and $T_{1/c}$=0.004, which represents a control filter that smooths out the signal from the inverter.

$$\Delta P_{pv} = \frac{1}{T_{pv}s + 1} \times \frac{1}{T_{in}s + 1} \times \frac{1}{T_{1/c} + 1} \tag{6}$$

The wind turbine can be represented as a first-order transfer function as given in (7) (Ibraheem et al., 2022). The time constant T_{WT}=1.5 defines how the wind turbine's power output responds to changes in the input signal. In LFC, this model regulates the active power output, manages the frequency response, and controls the pitch angle or rotor speed of the wind turbine to optimize power generation.

$$\Delta P_{WT} = \frac{1}{T_{WT}s + 1} \tag{7}$$

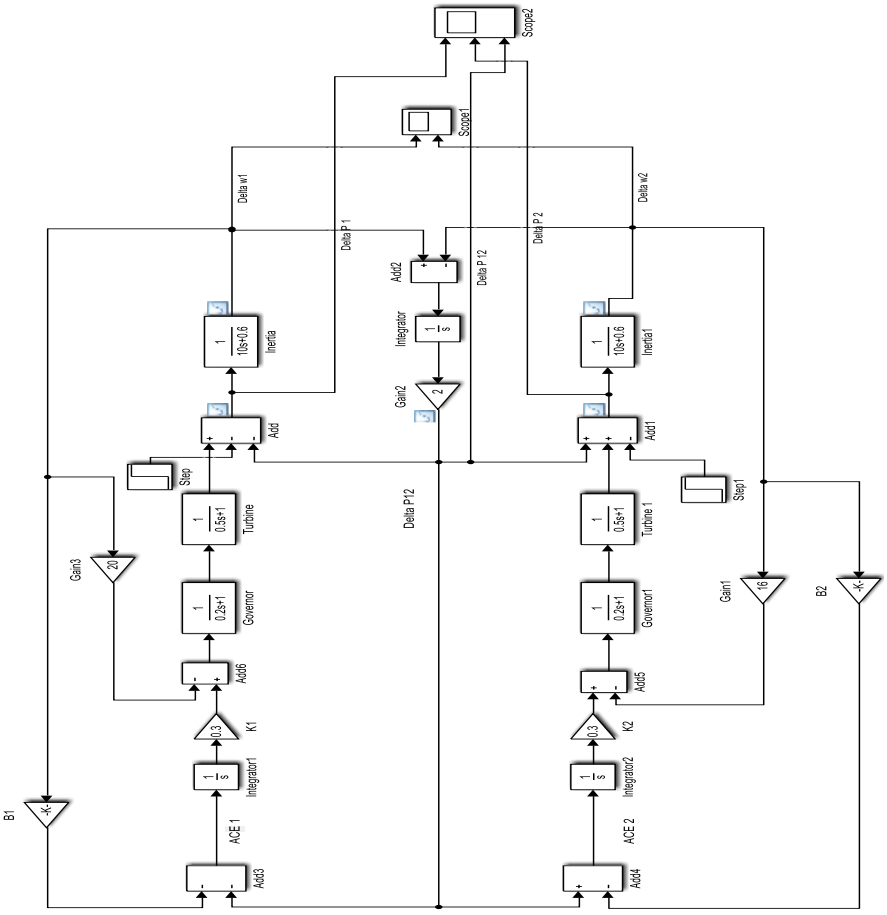

Figure 2. Transfer function representation of the two-area power system

2.4. Modeling of ESSs

For LFC studies, ESSs are considered ancillary services to provide or absorb active power to maintain system stability. The charging and discharging states are usually evaluated in contributing frequency stability. The change in the power output of BESS (ΔP_{BESS}) can be expressed as a first-order transfer function, given in (8) (Patel et al., 2019). The time constant of the BESS can be defined as T_{BESS}=0.1s. Similarly, the change in the power output of FESS (ΔP_{FESS}) can be expressed as a first-order transfer function, given in (9) (Ibraheem et al., 2022). For the flywheel energy storage system (FESS), the time constant T_{FESS} can be defined as 0.01s. For SMESS, (10) shows the change in the inductor voltage ΔE_d, where K_d=1 is the gain of the control loop and T_d=0.03s is the time delay associated with the power system converter (El-Saady et al., 2018).

$$\Delta P_{BESS} = \frac{1}{T_{BESS}s + 1} \tag{8}$$

$$\Delta P_{FESS} = \frac{1}{T_{FESS}s + 1} \tag{9}$$

$$\Delta E_d(s) = \frac{K_d}{T_d s + 1} \tag{10}$$

The deviation in the inductor current (ΔI_d) in SMESS can be calculated as in (11). L=2 Henry stands for the inductance of the SMESS coil. The deviation in the SMESS unit's power flow (ΔP_{SMES}) is shown in (12), where I_{do}=5A is the initial value of the inductor current.

$$\Delta I_d = \frac{\Delta E_d}{sL} \tag{11}$$

$$\Delta P_{SMES} = I_{do} \times \Delta E_d + \Delta E_d \times \Delta I_d \quad (12)$$

A comprehensive analysis of FESS, BESS, and SMESS is essential to understand their respective efficiencies, costs, and response times. This analysis enhances the practical value of energy storage studies by informing technology selection based on specific application requirements.

2.4.1. Comparative analysis of ESS

Each energy storage technology presents unique advantages and limitations. FESS offer high efficiency and rapid response but may incur higher costs depending on the materials used. BESS, particularly Li-ion batteries, provide high efficiencies and fast response times but are associated with significant capital cost. SMESS deliver exceptional efficiency and the fastest response times; however, their high cost can restrict their practical application. A detailed comparative analysis of these technologies is given in Table 2. Considering efficiency, cost, and response time, can significantly enhance the practical value of energy storage studies by guiding the selection of the most appropriate technology for specific applications.

Table 2. Comparative analysis of energy storage technologies

BESS	***FESS***	***SMESS***
• Efficiency: Lithium-ion (Li-ion) batteries, a common type of BESS, have efficiencies between 85% and 95% • Cost: the capital costs for BESS can be high, which impacts their economic viability. • Response Time: BESS can provide a fast response, making them suitable for various grid services, including frequency regulation and energy arbitrage (Jaffal et al., 2024). • Economics Impacts: Particularly lithium batteries, have seen significant cost reductions, enhancing their economic attractiveness. They provide benefits like grid stabilization, energy arbitrage, and deferred infrastructure investments. However, factors such a life span and degradation rates influence their overall economic viability. (Simpa et al., 2024) • Environmental Impacts: Production involves mining and processing of raw materials, leading to environmental concerns. Life cycle assessments indicate that lithium-ion batteries have life cycle greenhouse gas emissions ranging from 625 to 659kg-CO_2eq/MWh, depending on the application scenario. (Zhang et al., 2025)	• Efficiency: FESS typically exhibits high efficiencies, ranging from 90% to 95%. • Cost: the cost FESS varies depending on the materials used. For instance, a flywheel made from Carbon AS4C material cost approximately $313 for a 10kg unit. • Response Time: FESS is capable of rapid response times, making them suitable for applications requiring immediate power delivery (Altayf et al., 2024). • Economic Impacts: Typically have high initial capital costs due to advanced materials and precision engineering requirements. However, they offer long operational lifespans and minimal maintenance needs, potentially leading to favourable life cycle costs. • Environmental Impacts: FESS is environmentally friendly, as they do not involve chemical reactions, thereby eliminating risks of hazardous material leakage. Their primary environmental consideration is the energy consumed during manufacturing and operational losses. (Oskouei et al.,2022)	• Efficiency: SMESS is known for their high efficiencies, typically around 90% to 97%. • Cost: SMESS has relatively costs, which can be a limiting factor for widespread adoption. • Response Time: SMESS offers extremely rapid response times, often in the range of milliseconds, making them ideal for applications requiring instantaneous power delivery (Moradi-Shahrbabak and Jadidoleslam, 2023). • Environmental Impacts: the environmental footprint of SMESS is primarily associated with the production and maintenance of superconducting material and the energy requirements for cooling. While operational emissions are minimal, the overall environmental impact depends on the energy sources used for cooling and maintenance. • Economic Impacts: SMESS is characterized by high efficiency and rapid response time but entail substantial costs due to the need for superconducting materials and cryogenic cooling systems. These factors currently limit their widespread economic feasibility. (Lu, 2022)

2.5. Optimization methods

2.5.1. Artificial rabbit optimization (ARO)

ARO is a recently developed metaheuristic algorithm introduced in 2022. It draws inspiration from the foraging and hiding behavior of a real rabbit, incorporating their energy dynamics that facilitate transitions between these strategies (Wang et al., 2022b). One of the key strengths of ARO is its compliance with the global search convergence theorem, which guarantees that the algorithm will not overlook the global optimum during the search process. Consequently, ARO proves to be an efficient and reliable approach for solving complex optimization problems, as demonstrated in this study. The pseudocode of the ARO method is shown in Figure 3. This method can be utilized to optimize the PID controller parameters (Khalil et al., 2023). Rabbits prioritize distant areas and disregard nearby resources during the foraging, consuming grass randomly in other regions rather than their own. This behavior, termed "detour foraging," is emulated in the ARO algorithm. Each rabbit in the swarm is assumed to occupy its region containing grass and d burrows, while also visiting the positions of the other rabbits randomly for foraging. In practice, rabbits tend to explore around a food source to secure sufficient sustenance. Consequently, the detour foraging behavior in ARO reflects the tendency of each search agent to update its position toward a randomly selected individual within the swarm, incorporating a perturbation for variability (Khalil et al., 2023). The mathematical representation of this behavior is as follows:

$$\vec{V}_i(t+1) = \vec{x_j}(t) + R \cdot \left(\vec{x_i}(t) - \vec{x_j}(t)\right) + round\left(0.5 \cdot (0.05 + r_1)\right) \cdot n_1, i, j = 1, \dots, n \; and \; j \neq i \quad (13)$$

$$R = L \cdot c \quad (14)$$

$$L = \left(e - e^{\left(\frac{t-1}{T}\right)^2}\right) \cdot sin2\pi r_2 \quad (15)$$

$$c(k) = \begin{cases} 1, & if \; k == g(l) \\ 0, & else \end{cases} \qquad k = 1, \dots, d \; and \; l = 1, \dots, [r_3 \cdot d] \quad (16)$$

$$g = randperm(d) \quad (17)$$

$$n_1 \sim N(0,1) \quad (18)$$

where $\vec{V}_i(t+1)$is the candidate position of the i^{th} rabbit at the time t+1, while $\vec{x_j}(t)$ represents its position at iteration t. *n* represents the total number of the rabbit population, *d* corresponds to the dimension of the problem. T is the maximum number of the iteration, [·] is the ceiling function, round indicates rounding to the nearest integer, randperm returns a random permutation of the integers from 1 to *d.* Additionally, $r_1, r_2, and \; r_3$ are three random numbers in the range of (0,1). The parameter L denotes the running length, which quantifies the step size when performing the detour foraging, and . n_1 follows a standard normal distribution.

In (13), the perturbation may assist ARO to avoid local extrema and perform a global search. And (15), the running length L, can generate a longer step during the initial iterations. It selects one of the burrows for hiding to decrease the probability of being attacked. To escape from predators, a rabbit typically digs multiple burrows around its nest as potential hiding spots. In this algorithm, at each iteration, a rabbit always constructs *d* burrows along each dimension of the search space. The j^{th} burrow of the i^{th}rabbit is generated by.

$$\overrightarrow{b_{i,j}} = \vec{x_i}(t) + H.g.\vec{x_i}(t), i = 1, \dots, n \; and \; j = 1, \dots, d \quad (19)$$

$$H = \frac{T - t + 1}{T} \cdot r_4 \quad (20)$$

$$n_2 \sim N(0,1) \quad (21)$$

$$g(k) = \begin{cases} 1, & if \; k == j \\ 0, & else \end{cases} \qquad k = 1, \dots, d \quad (22)$$

According to (19), the d burrows are generated within the proximity of a rabbit along each dimension. H is the hiding parameter which decreases linearly from 1 to 1/T over the course of iteration, incorporating a random perturbation. Initially, these burrows are generated in a bigger neighborhood around the rabbit. However, as the iterations rise, this neighborhood shrinks too.

In the wildlife of a rabbit, a chase is a norm, so to survive, the rabbit needs a hiding place. As a result, they are inclined to stochastically select a burrow from their burrows for sheltering to avoid getting caught. The hiding strategy can be formulated mathematically from (23-25).

$$\overrightarrow{v_i}(t+1) = \overrightarrow{x_i}(t) + R.\left(r_4.\overrightarrow{b_{i,r}}(t) - \overrightarrow{x_i}(t)\right), i = 1, \dots, n \tag{23}$$

$$g_r(k) = \begin{cases} 1, & if\ k == [r_5.d] \\ 0, & else \end{cases} \qquad k = 1, \dots, d \tag{24}$$

$$\overrightarrow{b_{i,r}}(t) = \overrightarrow{x_i}(t) + H.g_r.\overrightarrow{x_i}(t) \tag{25}$$

Here, $\overrightarrow{b_{i,r}}$ denotes a randomly selected burrow for hiding among the d available burrows, and $r_4\ and\ r_5$are two random numbers in (0,1). Based on (23), the i^{th}Search individual attempts to update its position toward the selected burrow.

After one of both detour foraging and random hiding is achieved, i^{th} rabbit will be updated as follows:

$$\overrightarrow{x_i}(t+1) = \begin{cases} \overrightarrow{x_i}(t), & f(\overrightarrow{x_i}(t)) \le f(\overrightarrow{v_i}(t+1)) \\ \overrightarrow{v_i}(t+1), & f(\overrightarrow{x_i}(t)) > f(\overrightarrow{v_i}(t+1)) \end{cases} \tag{26}$$

In ARO, at the initial phase, rabbits often conduct detour foraging while frequently performing random hiding in the later phase of iteration. The energy of the rabbit is what drives the mechanism but it shrinks over the course of the iterations. Therefore, the energy factor in ARO is formulated as follows:

$$A(t) = 4\left(1 - \frac{t}{T}\right)\ln\frac{1}{r} \tag{27}$$

An energy factor is calculated to regulate the transition from exploration to exploitation in ARO. The parameter r represents a random variable. In ARO, when the energy factor $A(t) > 1$, the rabbit tends to search different foraging spaces randomly within the phase of the exploration.

Randomly initialize a set of rabbits Xi (solutions) and evaluate their fitness $F_i t_i$ and X_{best} is the best solution found so far
While the stop criterion is not satisfied do
For each individual Xi do
Calculate the energy factor A using Eq. (27).
If $A > 1$
Choose a rabbit randomly from other individuals.
Calculation R using $Eqs.$ (14)-(18)
Perform detour foraging using Eq. (13)
Calculate the fitness $F_i t_i$
Update the position of the current individual using Eq. (26)
Else
Generate d burrows and randomly pick one as hiding using Eq. (25)
Perform random hiding using Eq. (23).
Calculate the $F_i t_i$
Update the position of the individual using Eq. (26).
End if
Update the best solution found so far X_{best}
End For
End While
Return X_{best}

Figure 3. The pseudocode of the ARO method

2.5.2. Lightning search algorithm (LSA)

One of the newest metaheuristic algorithms developed by Shareef et al., (2015) has been crafted from the lightning phenomenon. The application of this method is cast across numerous fields of research and inventions such as computer science, engineering, and mathematics, to mention but a few. The idea of lightning can be attributed to the gaseous atoms namely; nitrogen, oxygen, and hydrogen in the thundercloud. As water molecules freeze within the thundercloud, the parts that cannot incorporate into the lattice, are propelled at high velocities. Imagine these ejected particles as tiny seeds "Just as seeds provide the foundation for plant development, these high-speed projectiles create the initial ionized channel that facilitates the step leader's progression, ultimately leading to a lightning strike". As they travel through the air, they collide with other molecules, creating a pathway for the lightning bolt to follow. This initial pathway is like the first step in creating the lightning bolt, similar to how the first seeds planted in a field are the starting point for a garden. The flowchart of the LSA is given in Figure 4.

$$V_p = [1 - (\frac{1}{\sqrt{1 - \left(\frac{V_0}{c}\right)^2}} - sf_i/mc^2)^{-2}]^{-1/2} \tag{28}$$

Where V_p and V_0 are the final and initial velocity of the projectile; c is the speed of light; f_i is the constant ionization rate; m is the mass of the projectile; and s is the length of the path traveled. Equation (28) proves that the projectile velocity is a function of leader tip position and projectile mass. Henceforth, Hydrogen with the lower atomic mass has little potential to ionize or explore a large space compared to Oxygen. Therefore, the exploration and exploitation capabilities of the algorithm can be guided using the relative energies of the step leaders.

To improve the algorithm's exploration capabilities, the concept of "forking" is designed. Projectile emits two symmetrical channels similar to the phenomenon of lightning forking. In this algorithm, forking is defined in two ways. Equation (29) presents the mathematical expression of the symmetrical channels that define nuclei collision which leads to the creation of symmetrical channels.

$$\overrightarrow{p_i} = x + y - p_i \tag{29}$$

Where $\overrightarrow{p_i}$ and p_i are the opposite and original projectiles, and x and y are the boundary limits in one dimension. This mechanism aims to improve the quality of less successful solutions within the population. Otherwise, one of the channels at the forking tip emerges to balance the c. Equation (30) demonstrates that the shaping parameter (α) exerts a significant influence over the trajectory. In the lightning search algorithm, the value of α for a specific space projectile $p^s$is dynamically determined by its distance from the current lead projectile P^l. This distance-dependent relationship directly influences the movement of the space projectile, as expressed;

$$p^s_{i_{new}} = p^s_i \pm exprand(\alpha_i) \tag{30}$$

If the calculated new position P^s_{new} of the space projectile is negative, it indicates a movement in the opposite direction. However, simply moving in the opposite direction doesn't guarantee successful channel formation. For successful propagation, the space projectile's energy $E^s_{p^i}$ must exceed the energy of the existing step leader E^{sl}_i. Only then can the space projectile extend the existing channel. If the new position $P^s_{i^{new}}$ leads to a successful channel extension, the corresponding step leader s^l_i is extended to this new position, and the space projectile's position is updated accordingly. Otherwise, both the space projectile and the step leader remain in their previous positions. If a particular space projectile successfully extends the step leader beyond the current longest leader in the system, it is then designated as the new lead projectile. Following Shareef et al., (2015), Analogous to the generation of space projectiles, the position of the lead projectile can be updated probabilistically. This update incorporates a random component generated from a normal distribution. The probability density function of the normal distribution can be expressed as:

$$f(x^l) = \frac{1}{\sigma\sqrt{n\pi}} e^{-\frac{(x^l-\alpha)\hat{}2}{2\sigma^2}} \quad (31)$$

Equation (31) demonstrates that the shaping parameter (α) significantly influences the directional exploration of the space projectile. In the LSA context, the parameter α^i for a specific space projectile P_i^s is dynamically determined by its proximity to the current lead projectile. This distance-dependent parameter governs the search behavior of the space projectile, influencing its movement within the solution space. The position of the space projectile P_i^s as shown in (32) at the subsequent step can be mathematically expressed as

$$P_{i_{new}}^L = p_i^l \pm normrand(\mu_L, \sigma_L) \quad (32)$$

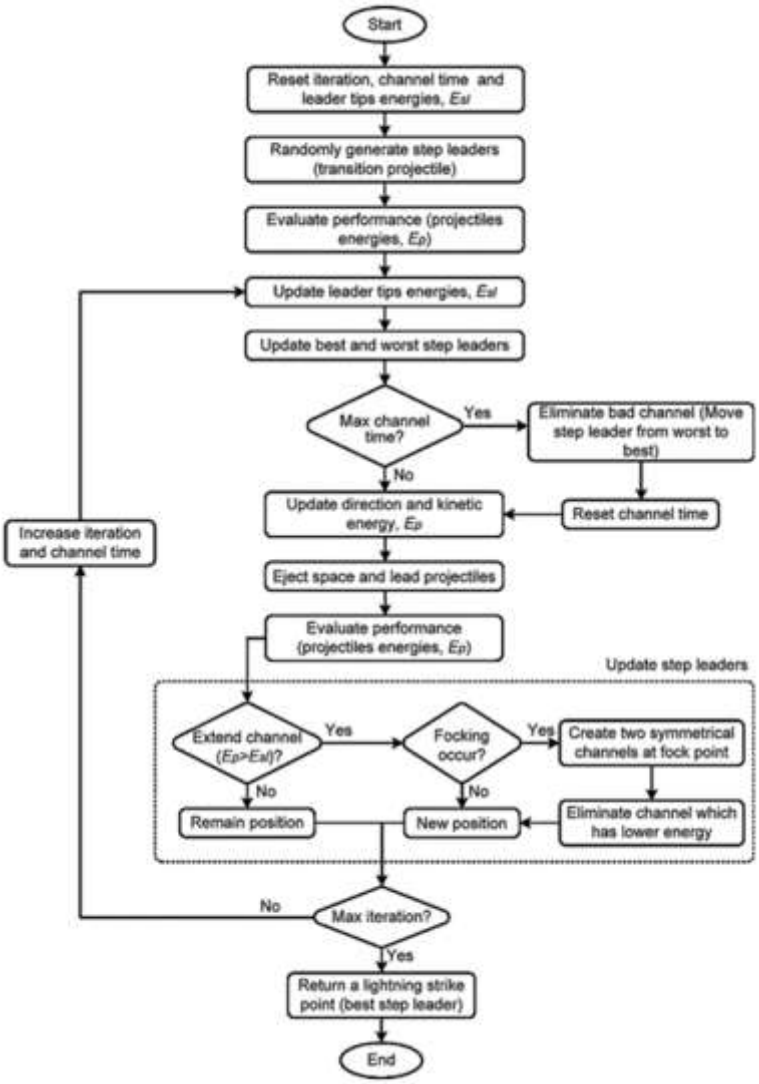

Figure 4. Flowchart of the LSA (Shareef et al., 2015)

2.5.3. Whale optimization algorithm (WOA)

Humpback whales' bubble-net feeding is a stunning display of cooperation and ingenuity in the natural world, as illustrated in Figure 5. This fascinating behavior involves whales diving beneath a school of fish and swimming in a spiral while releasing bubbles, creating a net that corrals the fish and forces them towards the surface. Inspired by this remarkable feeding strategy, WOA has been developed as a computational technique to solve complex optimization problems (Mirjalili and Lewis, 2016). This algorithm is designed based on the nature and tactics used by a whale to hunt and can be classified into three methodologies: encircling prey, bubble-net

attacking method, and searching for prey. These methodologies were used in designing the algorithm based on the following equations:

$$\vec{P} = \left|\overrightarrow{Q} \cdot \overrightarrow{R} * (t) - \vec{R}(t)\right| \tag{33}$$

$$\vec{R}(t+1) = \vec{R} * (t) - \vec{V} \cdot \overrightarrow{W} \tag{34}$$

where t denotes the current iteration, the vectors 'V' and 'Q' are coefficient vectors that dynamically adjust throughout the optimization process. 'R' represents the position vector of the current best solution within the search space. The operation '| |' signifies the absolute value, while '·' Denotes element-wise multiplication. It is crucial to note that the 'R' vector must be updated iteratively to reflect the discovery of any superior solutions during the optimization process.

$$\vec{V} = 2\vec{a} \cdot \vec{r} - \vec{a} \tag{35}$$

$$\vec{Q} = 2 \cdot \vec{r} \tag{36}$$

where $\vec{r}$ is a random vector, and $\vec{a}$ is linearly decreasing within the iteration from 2 to 0. The WOA mimics the bubble-net feeding behavior by employing mathematical models to simulate the whales' spiral and bubble-net patterns, effectively navigating through a search space to locate optimal solutions. This tactic can be categorized into two ways; shrinking encircling or spiral updating position. Just as the whales' coordinated efforts result in successful feeding, the WOA's iterative process and intelligent mechanisms aim to achieve high-quality solutions in various scientific and engineering applications. The pseudo-code of the WOA algorithm is given in Figure 6 (Mirjalili and Lewis, 2016).

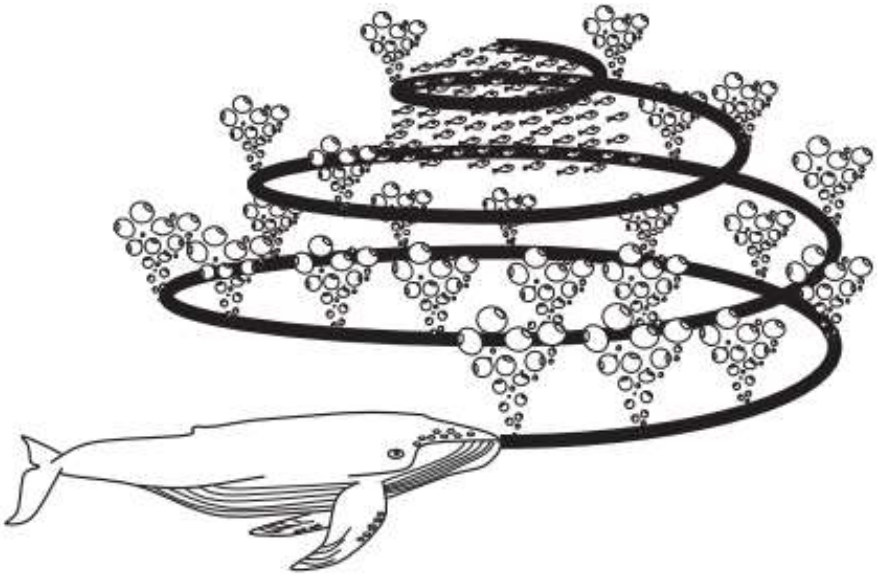

Figure 5. A bubble-net feeding behavior of humpback whales (Mirjalili and Lewis, 2016)

Shrinking encircling tactic is achieved by gradually reducing the magnitude of the coefficient vector 'V' in (35). Concurrently, the range of possible values for 'V' is also diminished by a factor of 'a' within the interval [-a, a], where the value of 'a' decreases linearly from 2 to 0 throughout the iterative process. The search space is progressively narrowed down by confining the value of 'a' within this decreasing range. Consequently, the new position of a search agent can be determined within a region bounded by its original position and the position of the current best solution. The potential positions are within the bounded region for a two-dimensional space. Assuming $0 \leq V \leq 1$. Spiral updating position tactic is inspired by the unique foraging behavior of humpback whales. This phase involves calculating the Euclidean distance between the current position of the whale (R, Y) and the position of the prey (R, Y). Subsequently, a spiral equation is derived to simulate the helical movement of the whale toward the prey, mirroring the observed behavior of humpback whales during bubble-net feeding.

$$\vec{R}(t+1) = \overrightarrow{W}.e^{bl}.\cos(2\pi l) + \vec{R} * (t) \tag{37}$$

Where $\vec{P} = |\vec{R} * (t) - \vec{R}(t)|$ and indicate the distance of the i^{th} whale to prey, b is a constant that defines the shape of the spiral, *l* is a stochastic number in [-1,1], and. is an element-by-element product.

The exploration phase of the WOA leverages variations in the V vector to simulate the process of prey searching. Humpback whales exhibit random search patterns based on their relative positions. In this context, V values greater than 1 or less than -1 are employed to drive search agents away from a reference whale, promoting diverse exploration. Unlike the exploitation phase, where the search agent updates their positions relative to the best solution found, the exploration phase updates based on a randomly selected search agent. This mechanism, combined with the condition $|\vec{V}|$ >1, enhances global search capabilities, ensuring broader exploration of the solution space. The corresponding mathematical model is as follows:

$$\vec{P} = \left|\vec{Q}.\overrightarrow{R_{rand}} - \vec{R}\right| \quad (38)$$

$$\vec{R}(t+1) = \overrightarrow{R_{rand}} - \vec{V}.\vec{P} \quad (39)$$

where $\overrightarrow{R_{rand}}$ is a random position vector chosen from the current position

Initialize the whale population Ri (i = 1, 2, ..., n)
Calculate the fitness of each search agent
R=the best search agent*
***While** (t < maximum number of iterations)*
  For each search agent
  Update V, w, C l, and a
    ***if 1** (w<0.5)*
      ***if 2** (|V| < 1)*
        Update the position of the current search agent by Eq. (33)
      ***Else if 2** (|V| ≥ 1)*
        Select a random search agent (R_{rand})
        Update the position of the current search agent by Eq. (39)
      End if 2
    ***Else if 1** (w≥0.5)*
        Update the position of the current search agent by Eq. (37)
    End if 1
  End for
  Check if any search agent goes beyond the search space, and amend it
  Calculate the fitness of each search agent
  Update R if there is a better solution*
  t=t+1
end while
*return R**

Figure 6. Pseudo-code of the WOA algorithm (Mirjalili and Lewis, 2016)

3. Results and Discussion

3.1. Case 1

In this case study, the single area-system is operated with a conventional PID controller ($K_p = 8.6147, K_i = 10, K_D = 4.1436$) without any RES or ESS integration. This system is simulated under a perturbation of step load change of 0.2 p.u applied at 0 second. The comparison of the system's change in frequency with and

without PID controller is shown in Figure 7. It is noted that the system frequency has a steady-state value of -0.0096 p.u. at 9.6 seconds when the PID controller is not activated. With the proper tuning of the PID controller, zero steady-state error in frequency change is attained at 12 seconds. Figure 8 shows that the system's power output is stabilized at 0.2 p.u. in a duration of around 8.3 seconds, which is equivalent to the load demand. Without PID controller, it is observed that the system's power output remains below the load demand.

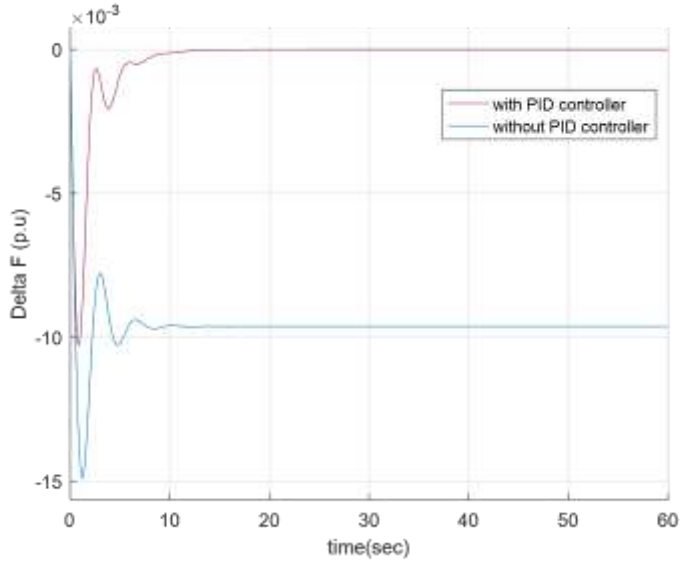

Figure 7. Comparison of the system's change in frequency with and without PID controller

Figure 7 presents the frequency deviation of the single-area under the influence of the PID controller, and the equivalent power output deviation under the same PID parameters is depicted in Figure 8.

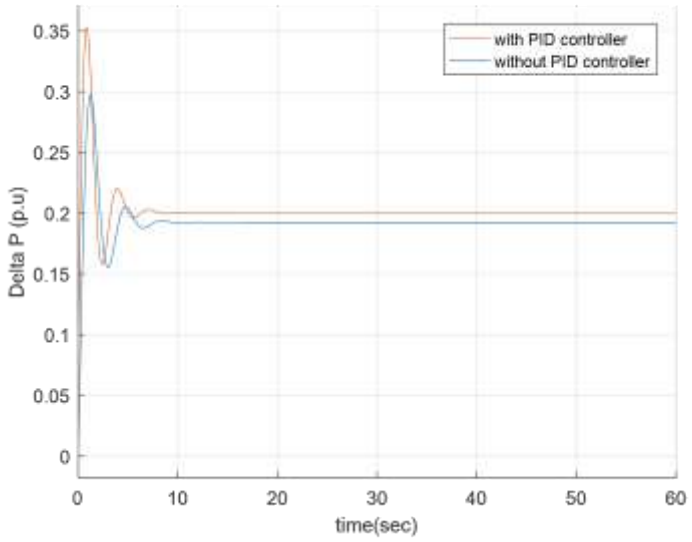

Figure 8. Comparison of the power output of the system with and without PID controller

It is clearly noted that the difference resulted in the output frequency and power stability at the nominal value in the shortest possible time due to the tuning effect of the PID controller. PID Tuning is important and an easier way to find the proper PID values.

3.2. Case 2

In this case study, PV and WT systems are added to the single-area system as shown in Figure 9. The system is exposed to severe load and irradiation variations as shown in Figure 10. At 2 s, the load increases from 0 to 0.1

p.u, then at 10 s, it drops to -0.05 p.u. The PID controller parameters are optimized using the aforementioned optimization methods (ARO, LSA, and WOA) which are simulated for 100 iterations, with 0 as the lower boundary and 10 as the upper boundary. For all, the population size is set as 50. The optimization results are presented in Table 3 when only PV system is activated. On the other hand, Table 4 shows the optimization results when only WT system is enabled. The optimization methods give the lowest settling time of 22.1 s for PV compared to 22.7 s for WT. Figure 11 compares three optimization methods for PID parameter tuning under constant irradiation. On the other hand, Figure 12 compares three optimization methods for PID parameter tuning under constant WT and variable load. In these figures, at 2s, the system experiences a big overshoot and the subsequent drop and a small overshoot at 10 s. ARO tuned PID controller causes fewer oscillations, the least settling time, and the smallest overshoot.

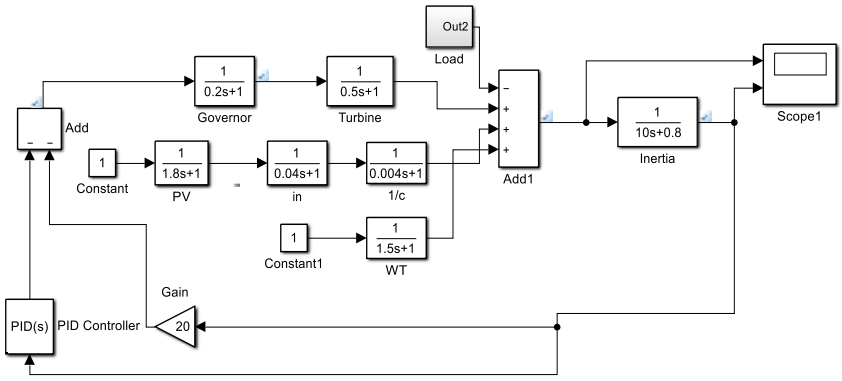

Figure 9. Transfer function representation of the single-area system with PV and WT integration

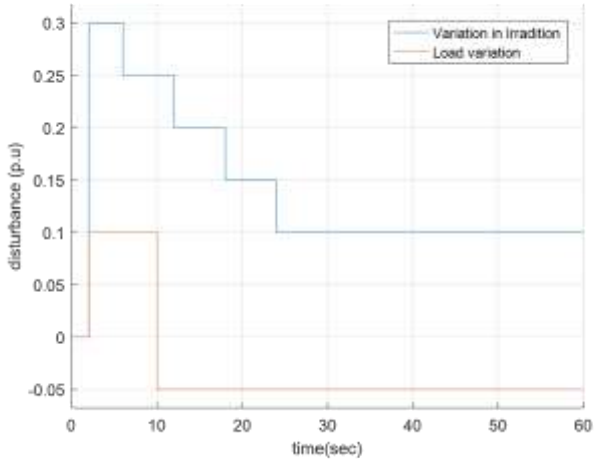

Figure 10. Load and irradiation variation applied to the system

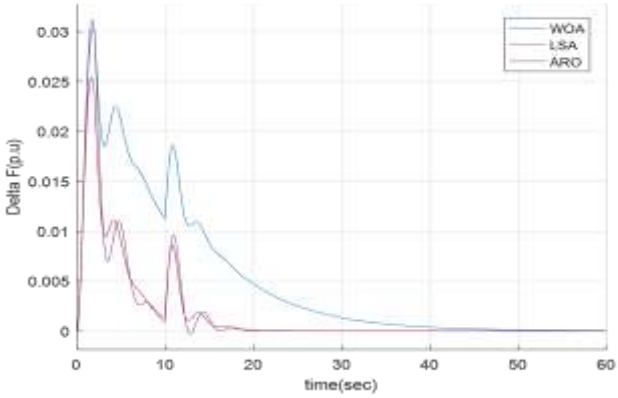

Figure 11. Comparison of ARO, LSA, and WOA under constant irradiation

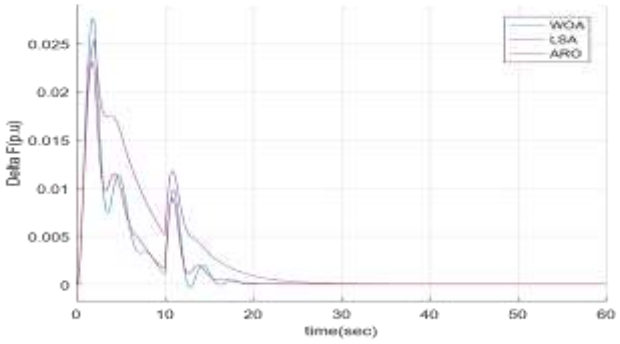

Figure 12. Comparison of ARO, LSA, and WOA under constant WT and variable load

Table 3. Optimization results for PID parameters for single-area system under constant irradiation

Optimization method	ITAE	Overshoot	undershoot	Settling time	PID parameters (K, K_i, and K_d)
ARO	0.5494	0.023	0	22.1	8.6147, 10, 4.1436
WOA	0.5269	0.028	-0.00038	22.1	4.7109, 9.8305, 1.7877
LSA	1.194	0.025	0	34	5.8375, 5.9462, 5.6458

Table 4. Optimization results for PID parameters for single-area system under constant wind speed

Optimization method	ITAE	Overshoot	Undershoot	Settling time	PID parameters (K, K_i, and K_d)
ARO	0.5174	0.025	0	22.7	8.8427, 10, 4.3477
WOA	3.21	0.0301	0	60	7.5469, 3.3712, 2.3995
LSA	0.5147	0.0312	0	23.2	4.3118, 9.4766, 1.8173

3.3. Case 3

The performance of the three optimization algorithms ARO, WOA, and LSA has been evaluated for a single-area power system integrated with constant PV and WT. The simulation results, shown in Table 5, highlighted the effectiveness of each optimization method in enhancing the system's stability by minimizing frequency deviations caused by load disturbances. ARO achieved the lowest integral time absolute error (ITAE) value of 0.5985, indicating superior performance in reducing the overall system error. Undershoot and overshoot are critical in evaluating system stability, as they indicate how much the system deviates from the desired steady-state frequency. While WOA has the lowest undershoot, the balance between undershoot and overshoot makes ARO more favorable in terms of overall stability. The proportional and integral gains are higher in ARO which contributes to faster system stability, while the derivative is tuned to reduce oscillations. Figure 13 shows the ARO curve with minimal oscillations and achieves steady-state frequency faster than the other two.

3.4. Case 4

The wind turbine is considered to have an input of white noise generating random numbers. This is closer to reality since the wind blows continuously and is unstable as shown in Figure 14. The solar irradiation is

increased to 0.3 p.u at 2 s according to Figure 13, and then began to decrease by -0.05 p.u step by step at 6, 12, 18, and 24 s until it is reduced to 0.1 p.u. Figure 15, shows the frequency response of the system, and all optimization methods respond well especially ARO as it shows better damping of oscillations compared to WOA and LSA, indicating faster adaptation to random noise and solar variations, and better frequency stability during the stepwise decrease in solar irradiation. LSA struggles to handle the noise effectively, leading to large and more persistent oscillation. WOA performs moderately well but shows slightly higher oscillation.

Table 5. Optimization results for PID parameters for single-area system under constant irradiation and constant wind speed

Optimization method	ITAE	Undershoot $\times 10^{-3}$	Overshoot $\times 10^{-3}$	Settling time	PID parameters (K, K_i, and K_d)
ARO	0.5985	0.454	4.944	15.12	10, 10, 3.0713
WOA	0.9747	0.026	4.59	17.1	9.4301, 6.5550, 6.2250
LSA	4.285	7.5	2.61	39.1	3.1908, 5.9219, 7.7052

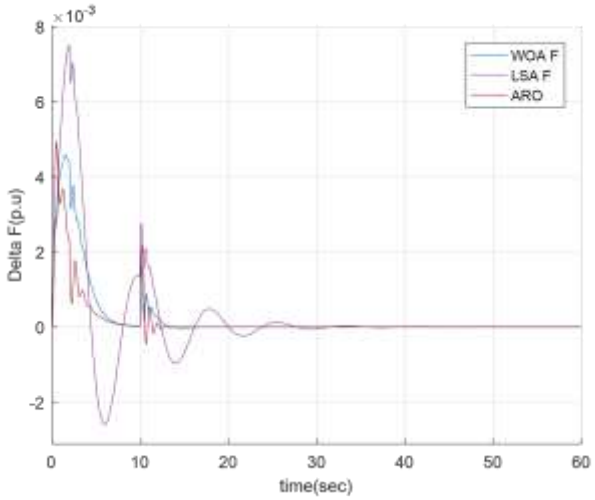

Figure 13. Comparison of ARO, WOA, and LSA under constant RES in a single–area system

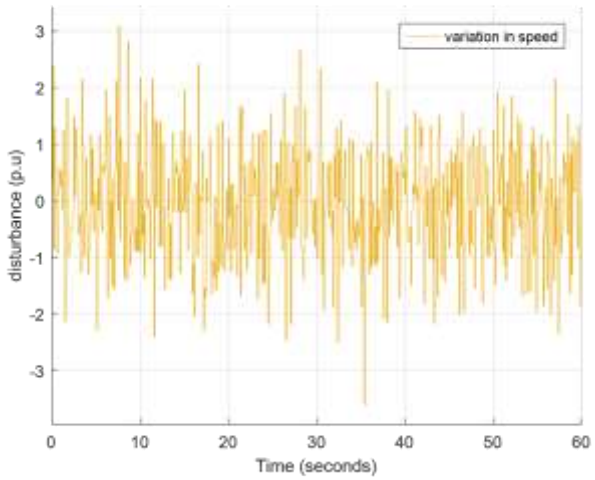

Figure 14. White noise is used as a variation in the speed of WT

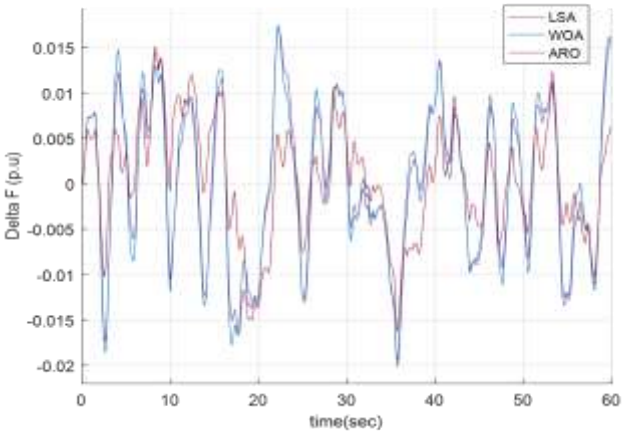

Figure 15. Comparison of ARO, LSA, and WOA under severe disturbances

3.5. Case 5

The two-area power system is simulated using the parameters listed in Table 1 in the following case studies. Several simulation scenarios are rendered to thoroughly investigate the system stability with respect to steady-state frequency and power output. The optimization performance of the aforementioned optimization methods on PID controller parameter tuning is also investigated. Different types of ESSs are employed in the system to play a stability control role. A load disturbance of 2% is applied in Area-1 and 1.5% in Area-2, each at 2 s. Figure 16 illustrates the steady-state frequency of the system in both areas. Long undershoots and short overshoots right at 2 s are observed, then the system reaches a steady-state condition at 21.8 s as indicated in Table 6. These results show the effectiveness of the LFC under an area control error strategy in which each load demand is compensated by the governor assigned to that area. On the other hand, Figure 17 shows the output power of the two-area system and the two overshoots at 2 s confirm the surge in the load in both areas. The subsequent steady-state at zero shows the system stability and effectiveness of the automatic LFC approach. To further enhance the system's stability and steady-state frequency, ESSs are tested to investigate their effects. Figures 18 and 19 present the steady-state frequency due to each ESS. Table 7 offers the performance indices, where the FESS has the shortest undershoot in both areas followed by BESS and then SMESS. The overshoots seem to die out except for SMESS, and the settling time is a disadvantage for all the ESSs. Figures 20 and 21 show the steady-state power output of both areas in response to the step load perturbation of 0.2 p.u for Area-1 delivered at 2 s and 0.15 p.u for Area-2 at 2 s. FESS shows a significant improvement in the overshoots of the system followed by BESS, SMESS as reported Table 7. However, the settling time is seen to be disadvantageous for the ESSs in both areas. in a nutshell, ESSs are seen to dampen the oscillations and increase the settling time. Figure 22 represents the tie-line steady-state power output due to the ESSs.

Table 6. Comparison of ESS performances on the two-area system

ESS type	**Overshoot× 10^{-3}**		**Undershoot× 10^{-3}**		**Settling time (s)**	
	Area-1	**Area-2**	**Area-1**	**Area-2**	**Area-1**	**Area-2**
No ESS	2.8	1.9	-14.6	-14.9	21.8	28.1
FESS	0	0	-8.3	-6.85	32.4	43.1
SMESS	0	-3	-10.1	-8.7	29.8	35.6
BESS	0	0	-8.8	-7.22	35.5	43.5

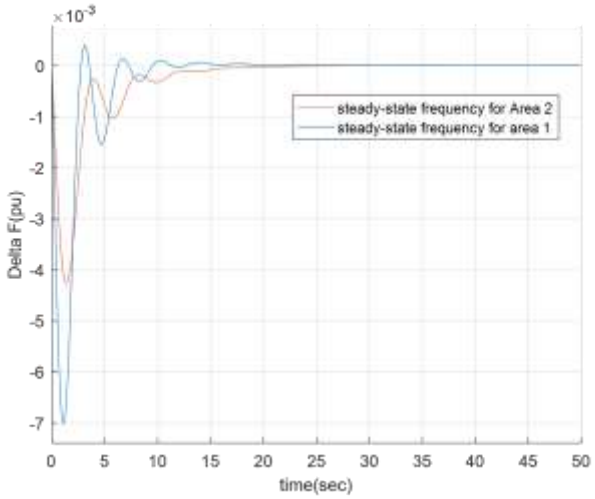

Figure 16. Frequency deviation of the system tested under different load surges in Areas 1-2

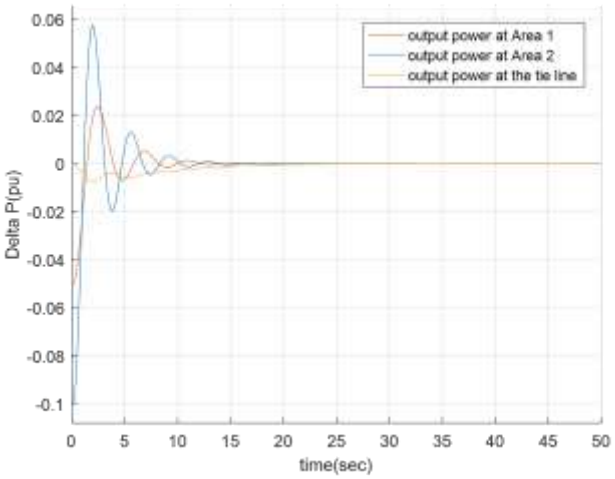

Figure 17. The power output produced by the two areas and the tie line

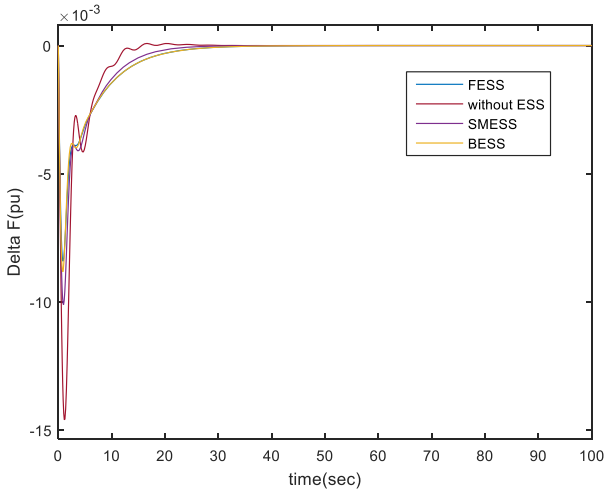

Figure 18. Comparison of the frequency deviation in Area-1 due to the ESS

Table 7. Comparison of power output parameters due to ESS

ESS type	Overshoot× 10^{-3}		Undershoot× 10^{-3}		Settling time (s)	
	Area-1	Area-2	Area-1	Area-2	Area-1	Area-2
No ESS	182	125	136	110	43.1	28.1
FESS	327	281	158	86	27.1	28.1
SMESS	220	159	148	120	35.6	28.1
BESS	187	127	132	107	43.1	28.1

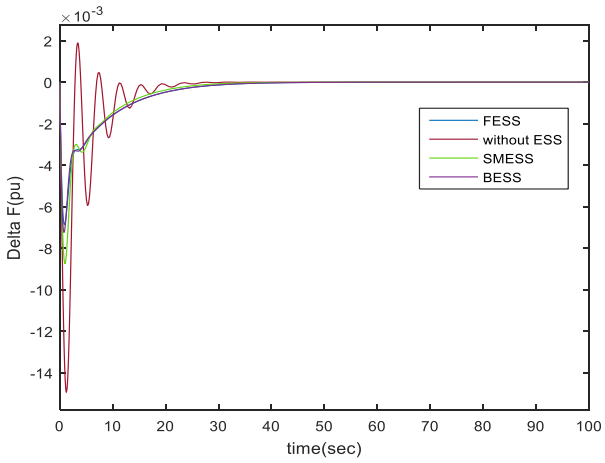

Figure 19. Comparison of frequency deviation in Area-2 due to ESS

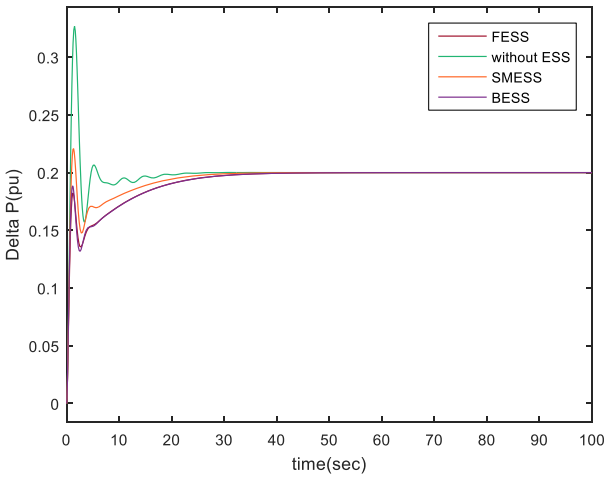

Figure 20. The power output due to ESS at Area-1

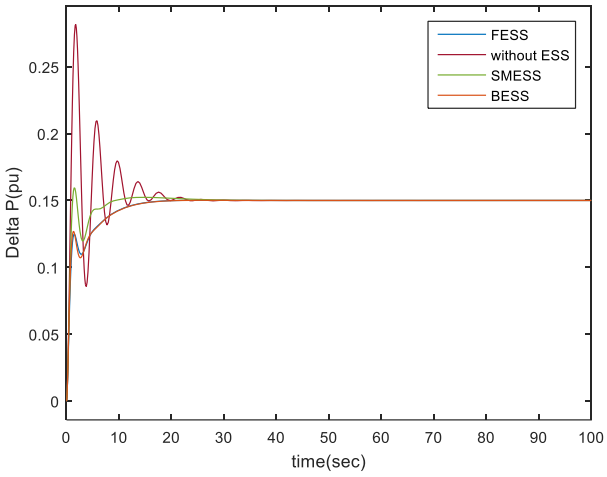

Figure 21. The power output due to ESS in Area-2

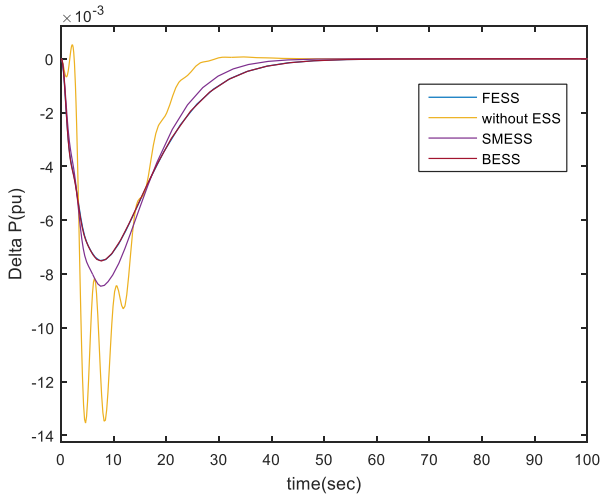

Figure 22. The tie-line steady-state power output due to the ESSs.

3.6. Case 6

RES, such as PV and WT systems, are activated in the two-area system. Figure 23 shows the model configuration. This study is evaluated based on the optimization techniques and the indices upon which the selection of the best technique depends is the popular error criteria namely "ITAE" and then the overshoot, undershoot as well as the settling time. The system responds to the significant load perturbation as illustrated in Figure 10. A load of 0.2 p.u delivered at 2s and the subsequent load value falls of 0.05 p.u. at 10 s. The overshoot at the corresponding times can be observed in Figures 24 and 25, representing Area-1 and 2. The ARO is seen to have a minimum ITAE of 0.2126 in Area-1 and 0.6035 in Area-2 compared to WOA and LSA as can be seen in Table 8. The ARO has also the least overshoot and undershoot in both areas. These results prove the superiority of ARO method on the overall basis compared to the LSA and WOA methods.

Table 8. Comparison of optimized parameters for the two-area system under constant RES

Optimization Method	ITAE1	ITAE2	Overshoot× 10^{-3}		Undershoot× 10^{-3}		Settling time (s)	
			Area-1	Area-2	Area-1	Area-2	Area-1	Area-2
LSA	0.4809	27.04	3.9	2.97	0	0	100	100
WOA	0.406	0.2221	8.1	3.93	-1.2	-0.24	16.9	26.4
ARO	0.2126	0.6035	2.4	2.22	-0.8	-0.42	29.8	21.4

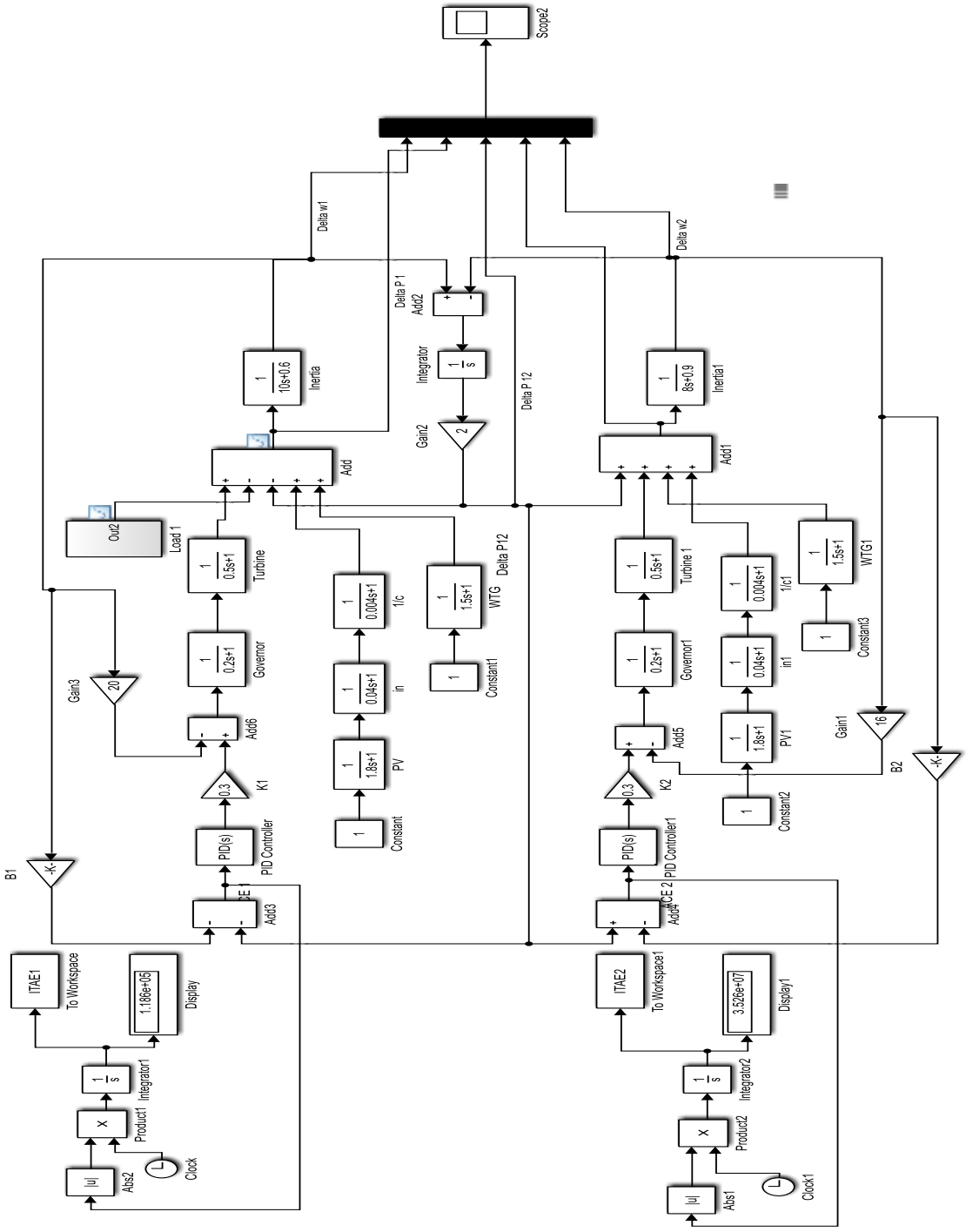

Figure 23. Renewable energy penetration with a constant input in both areas

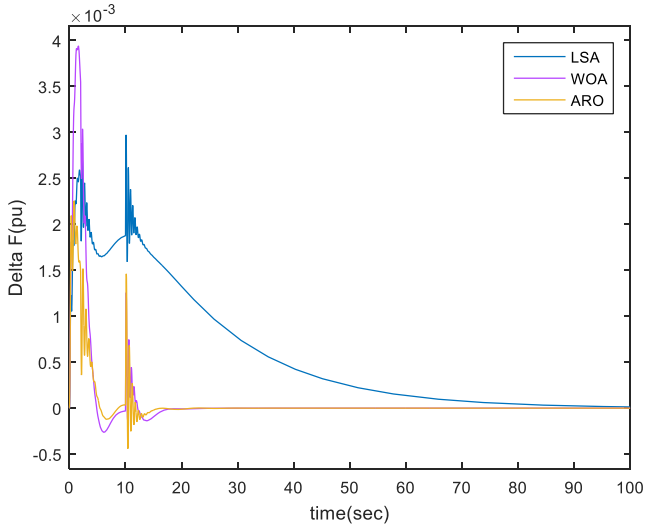

Figure 24. The frequency deviation of Area-1 under constant PV, WT, and variable load

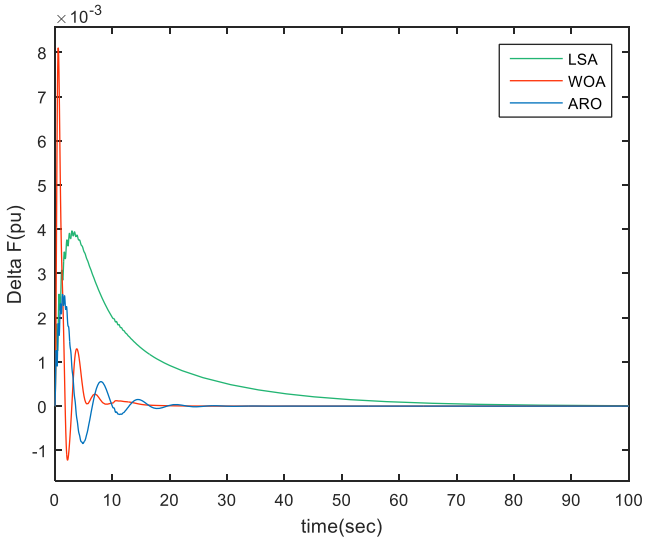

Figure 25. Comparison of frequency deviation of Area-2 under constant PV, WT, and no load

3.7. Case 7

The configuration of the overall system constituting PV, WT, and the load is shown in Figure 26. The main aim of this case is to examine the superiority of ARO in subduing a complex disturbance in the system due to the severe disturbances from the PV, WT, and the load as illustrated in Figure 27. The load surges at 2 s to 0.1 p.u and then drops to -0.05 p.u at 10 s. This fluctuation is reflected at the corresponding time in Figure 28 since the load is only applied to Area-1. Both PV and WT systems have a steady increment in disturbance of 0.05 p.u at 0,7,11,16 and 20 s. The only difference is that there is an abrupt fall of WT speed at 20 s to -0.05 p.u. Under these disturbances. The optimization techniques are applied to improve the PID controller parameters. Table 9 provides the quantitative analyses of Figures 28 and 29 which represent Area-1&2. The ARO method has the lowest ITAE of 0.3431 for Area-1 and 0.2642 for Area-2, providing a minimum settling time of 33.1 s.

Table 9. Parameters due to optimizations under variable load and ESS in both areas

Optimization Method	ITAE1	ITAE2	Undershoot× 10^{-4}		Overshoot× 10^{-4}		Settling time (s)	
			Area-1	Area-2	Area-1	Area-2	Area-1	Area-2
WOA	0.9458	0.5858	-10.3	-2.74	19.5	2.75	30.1	43.7
LSA	3.943	2.386	-5.6	-1.8	16.2	6.43	51.8	100
ARO	0.3431	0.2642	-9.5	-4.67	15.3	2.55	25	33.1

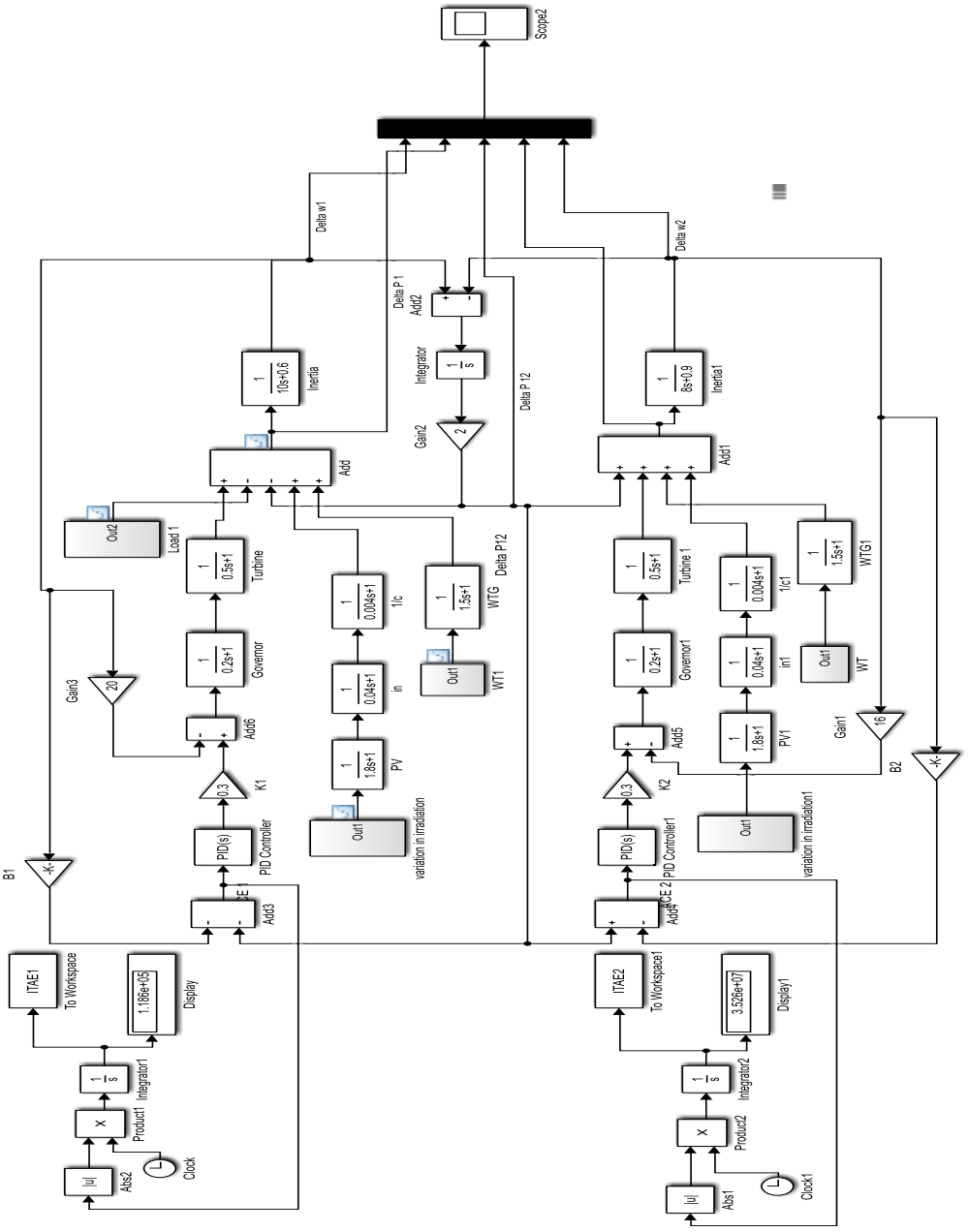

Figure 26. Integration of RES into the System model in both areas and Load disturbance in Area-1

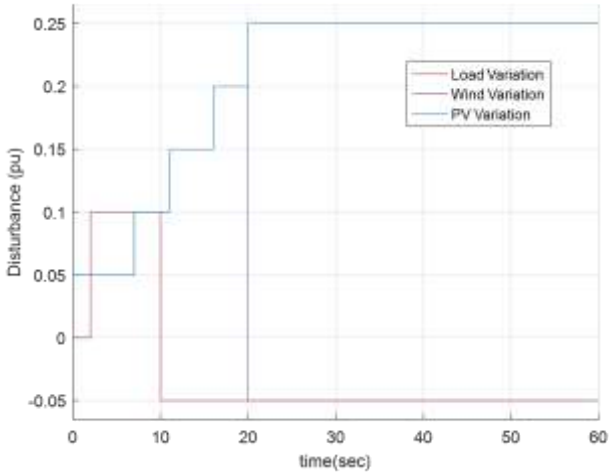

Figure 27. The disturbances applied to the system

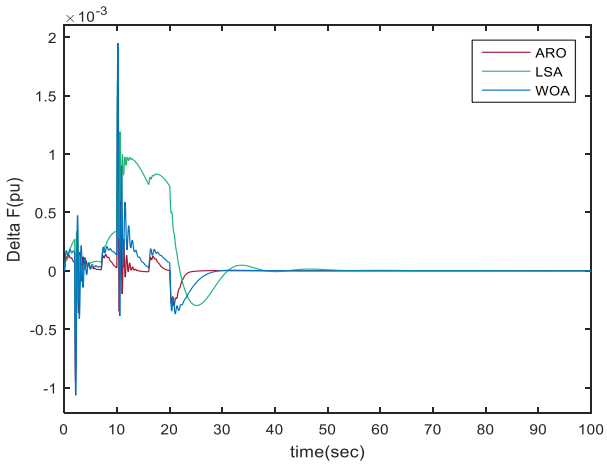

Figure 28. Comparison of frequency deviation optimizations in Area-1

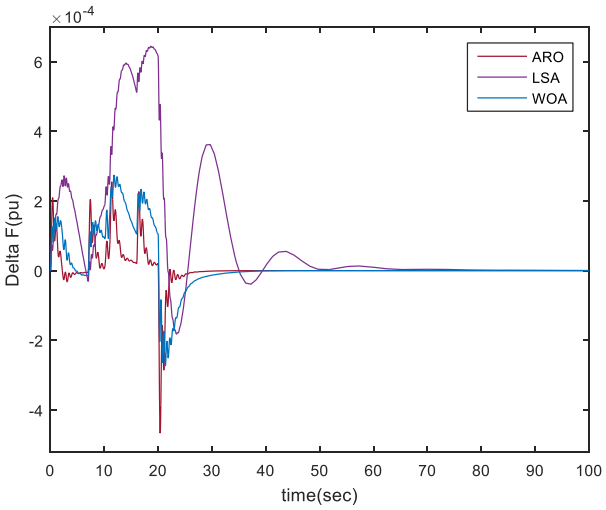

Figure 29. Comparison of frequency deviation optimizations in Area-2

3.8. Case 8

Under constant PV, WT, and variable load, the two-area system is tested by charging and discharging FESS. The responses are presented in Figures 30, 31, and 32. Also under variable load and RES conditions, the responses are illustrated in Figures 33, 34, and 35. Numerous research papers explore the technology of charging and discharging ESS. On the other hand, especially, FESS can be preferred due to its fast response and durability (Nguyen and Hoang, 2020). The smoother response of FESS in the charging phase can be compared to the discharging state. Both charging and discharging states are effective but the intrinsic characteristics of charging tend to result in smoother damping of oscillations (Canizares et al., 2021; Xie et al., 2023).

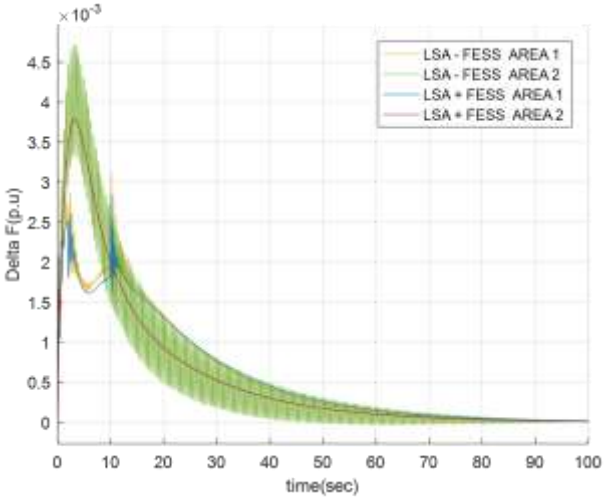

Figure 30. Frequency deviation comparison under LSA on charging and discharging of FESS

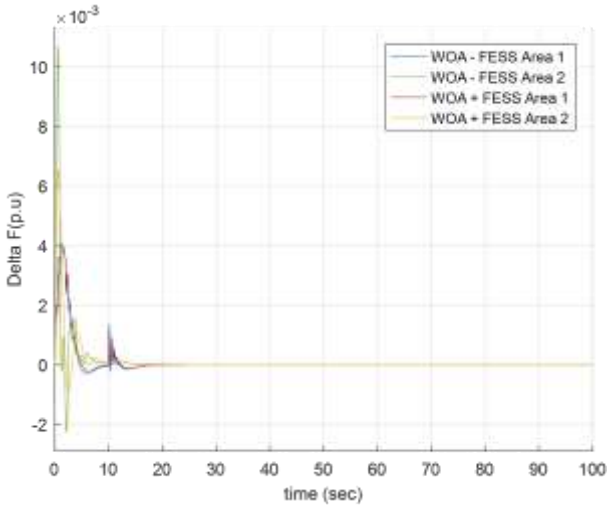

Figure 31. Frequency deviation comparison under WOA on charging and discharging of FESS

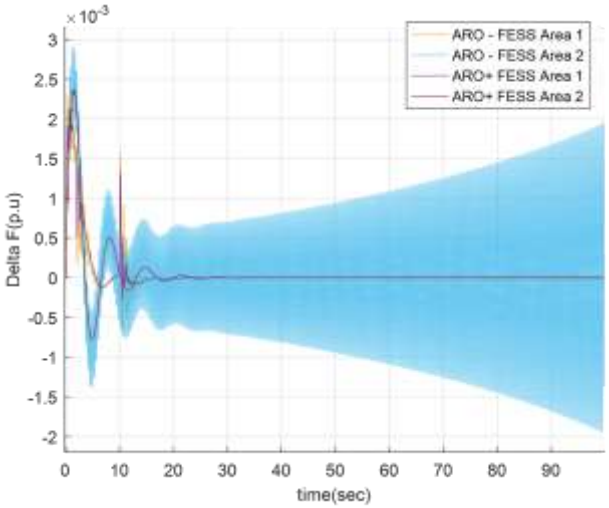

Figure 32. Frequency deviation comparison under ARO on charging and discharging of FESS

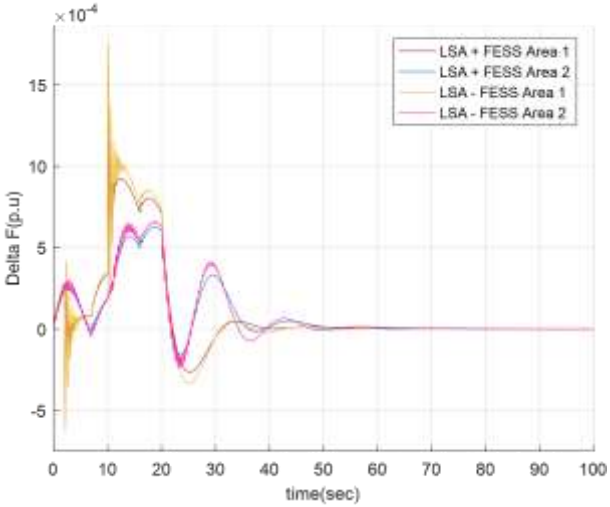

Figure 33. Frequency deviation comparison under LSA on charging and discharging of FESS

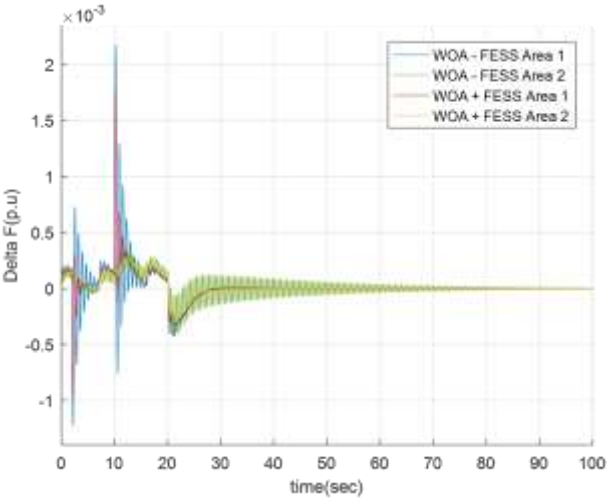

Figure 34. Frequency deviation comparison under WOA on charging and discharging of FESS

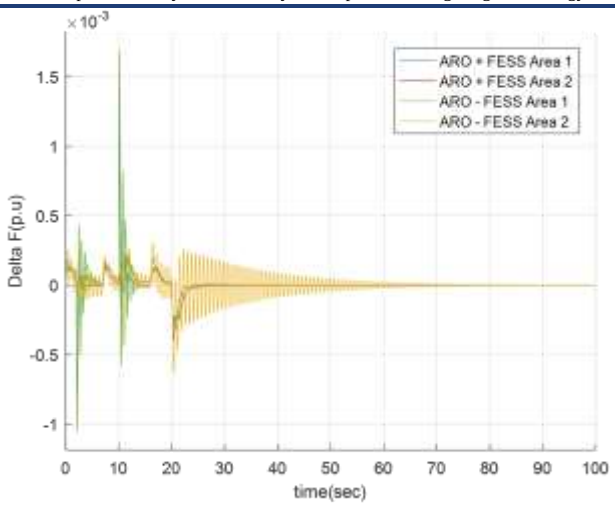

Figure 35. Frequency deviation comparison under ARO on charging and discharging of FESS

4. Conclusion

This study emphasizes the advantage of effective frequency regulation in modern power systems, especially with the increasing integration of RES, such as PV and WT systems. The variability and uncertainty in RES outputs, together with dynamic load changes, create significant challenges to maintaining system stability. This research evaluates the performance of three optimization methods (ARO, LSA, and WOA) to improve the tuning of PID controllers for frequency control in both single-area and two-area test systems. The findings demonstrate ARO's superior robustness in mitigating frequency instability caused by severe load perturbations and variable RES inputs. The study further highlights the impact of ESS such as BESS, FESS, and SMESS on system stability. The FESS stands out as the most effective ESS in reducing frequency oscillations and improving transient stability. However, all ESSs introduce a trade-off by increasing the system settling time. The combination of optimized PID control and ESS deployment offers a reliable solution to address the challenges posed by the variability of RES and dynamic load changes in power systems.

The overall deduction ascertains that there is no single “superior” energy storage system- each excels in different applications and economic feasibility. BESS has environmental concerns but is best for grid-scale energy storage. FESS has a high cost but supplies high power and a long lifespan. Finally, SMESS has high costs and cooling requirements but offers the highest efficiency.

Ethics Permissions

This paper does not require ethics committee approval.

Author Contributions

A. Garba Ibrahim conceived and designed the experiments; A. Mete Vural and A. Garba Ibrahim proposed the methods and analyzed the data; A. Garba Ibrahim drafted the manuscript. A. Mete Vural revised the manuscript and edited English language. All authors read and approved the final version.

Conflict of Interest

The authors declare that the research was conducted in the absence of any commercial or financial relationships that could be construed as a potential conflict of interest.

References

Akram, U., Nadarajah, M., Shah, R., and Milano, F. (2020). A review on rapid responsive energy storage technologies for frequency regulation in modern power systems. *Renewable and Sustainable Energy Reviews, 120*, 109626. https://doi.org/10.1016/j.rser.2019.109626

Ali, G., Aly, H., and Little, T. (2024). Automatic generation control of a multi-area hybrid renewable energy system using a proposed novel GA-fuzzy logic self-tuning PID controller. *Energies, 17*(9), 2000. https://doi.org/10.3390/en17092000

Altayf, A., Trabelsi, H., Hmad, J., and Benachaiba, C. (2024). Multi-criteria decision-making approach to the intelligent selection of PV-BESS based on cost and reliability. *International Journal of Energy Production and Management*, *9*(2), 83–96. https://doi.org/10.18280/ijepm.090203

Cañizares, C. A., E, N. S. G., Bhattacharya, K., andSohm, D. (2021). Frequency regulation model of bulk power systems with energy storage. *IEEE Transactions on Power Systems*, *37*(2), 913–926. https://doi.org/10.1109/TPWRS.2021.3108728

Hutchinson, A. J., Harrison, C. M., Bryden, T. S., Alahyari, A., Hu, Y., Gladwin, D. T., ... and Forsyth, A. (2025). A comprehensive review of modeling approaches for grid-connected energy storage technologies. *Journal of Energy Storage*, *109*, 115057. https://doi.org/10.1016/j.est.2024.115057

Cansiz, A., Faydaci, C., Qureshi, M. T., Usta, O., and McGuiness, D. T. (2017). Integration of a SMES–battery-based hybrid energy storage system into microgrids. *Journal of Superconductivity and Novel Magnetism*, *31*(5), 1449–1457. https://doi.org/10.1007/s10948-017-4338-4

El-Saady, G., Ibrahim, E. A., and Okilly, A. H. (2018). HVDC FACTS controller for load frequency control system. In *Proceedings of the Fourth International Conference on Energy Engineering (ICEE-4)*, Aswan University, Egypt.

Elsisi, M., Aboelela, M., Soliman, M., and Mansour, W. (2018). Design of optimal model predictive controller for LFC of nonlinear multi-area power system with energy storage devices. *Electric Power Components and Systems*, *46*(11–12), 1300–1311. https://doi.org/10.1080/15325008.2018.1469056

Georgious, R., Refaat, R., Garcia, J., and Daoud, A. A. (2021). Review on energy storage systems in microgrids. *Electronics*, *10*(17), 2134. https://doi.org/10.3390/electronics10172134

Hajiaghasi, S., Salemnia, A., and Hamzeh, M. (2019). Hybrid energy storage system for microgrids applications: A review. *Journal of Energy Storage*, *21*, 543–570. https://doi.org/10.1016/j.est.2018.12.017

Ibraheem, M. I., Edrisi, M., Gholipour, M., and Alhelou, H. H. (2022). A novel frequency regulation in islanded microgrid using sliding mode control with disturbance observers considering storages and EVs. *Computers and Electrical Engineering*, *105*, 108537. https://doi.org/10.1016/j.compeleceng.2022.108537

Chakraborty, M. R., Dawn, S., Saha, P. K., Basu, J. B., and Ustun, T. S. (2022). A comparative review on energy storage systems and their application in deregulated systems. *Batteries*, *8*(9), 124. https://doi.org/10.3390/batteries8090124

Ibrahim, L. O., In-Young, C., Jang, Y., Shim, J. W., Sung, Y. M., Yoon, M., and Suh, J. (2022). Coordinated frequency control of an energy storage system with a generator for frequency regulation in a power plant. *Sustainability*, *14*(24), 16933. https://doi.org/10.3390/su142416933

Jaffal, H., Guanetti, L., Rancilio, G., Spiller, M., Bovera, F., and Merlo, M. (2024). Battery energy storage system performance in providing various electricity market services. *Batteries*, *10*(3), 69. https://doi.org/10.3390/batteries10030069

Julius, A., Corigliano, S., Merlo, M., and Dan, Z. (2022). BESS primary frequency control strategies for West African power pool. *Energies*, *15*, 990. https://doi.org/10.3390/en15030990

Ramesh Kumar, S., and Ganapathy, S. (2013). Design of load frequency controllers for interconnected power systems with superconducting magnetic energy storage units using bat algorithm. *IOSR Journal of Electrical and Electronics Engineering*, *6*(4), 42–47.

Khalil, A. E., Boghdady, T. A., Alham, M. H., and Ibrahim, D. K. (2023). Enhancing the conventional controllers for load frequency control of isolated microgrids using proposed multi-objective formulation via artificial rabbits optimization algorithm. *IEEE Access*, *11*, 3472–3493. https://doi.org/10.1109/ACCESS.2023.3234043

Li, M., Shan, R., Abdullah, A., Tian, J., and Gao, S. (2023). High energy capacity or high energy rating: Which is the more important performance metric for battery energy storage systems at different penetrations of variable renewables? *Journal of Energy Storage*, *59*, 106560. https://doi.org/10.1016/j.est.2022.106560

Lin, X., and Zamora, R. (2022). Controls of hybrid energy storage systems in microgrids: Critical review, case study and future trends. *Journal of Energy Storage*, *47*, 103884. https://doi.org/10.1016/j.est.2021.103884

Lu, R. (2022). Sustainability and environmental efficiency of superconducting magnetic energy storage (SMES) technology. *Highlights in Science, Engineering and Technology*, *26*, 365–371. http://dx.doi.org/10.54097/hset.v26i.4005

McIlwaine, N., Foley, A. M., Kez, D. A., Best, R., Lu, X., and Zhang, C. (2021). A market assessment of distributed battery energy storage to facilitate higher renewable penetration in an isolated power system. *IEEE Access*, *10*, 2382–2398. https://doi.org/10.1109/ACCESS.2021.3139159

Mirjalili, S., and Lewis, A. (2016). The whale optimization algorithm. *Advances in Engineering Software, 95*, 51–67. https://doi.org/10.1016/j.advengsoft.2016.01.008

Moradi-Shahrbabak, Z., and Jadidoleslam, M. (2023). A new index for techno-economical comparison of storage technologies considering effect of self-discharge. *IET Renewable Power Generation, 17*, 1699–1712. https://doi.org/10.1049/rpg2.12704

Mugyema, M., Botha, C. D., Kamper, M. J., Wang, R.-J., and Sebitosi, A. B. (2023). Levelised cost of storage comparison of energy storage systems for use in primary response application. *Journal of Energy Storage, 59*, 106568. https://doi.org/10.1016/j.est.2022.106573

Nguyen, X. P., and Hoang, A. T. (2020). The flywheel energy storage system: An effective solution to accumulate renewable energy. In *2020 6th International Conference on Advanced Computing and Communication Systems (ICACCS)* (pp. 1322–1328). IEEE. https://doi.org/10.1109/ICACCS48705.2020.9074469

Nguyen-Huu, T., Nguyen, V. T., Hur, K., and Shim, J. W. (2020). Coordinated control of a hybrid energy storage system for improving the capability of frequency regulation and state-of-charge management. *Energies, 13*(23), 6304. https://doi.org/10.3390/en13236304

Oskouei, M. Z., Seker, A. A., Tunçel, S., Demirbaş, E., Gözel, T., Hocaoğlu, M. H., ... and Mohammadi-Ivatloo, B. (2022). A critical review on the impacts of energy storage systems and demand-side management strategies in the economic operation of renewable-based distribution network. *Sustainability, 14*, 2110. https://doi.org/10.3390/su14042110

Patel, V., Guha, D., and Purwar, S. (2019). Frequency regulation of an islanded microgrid using integral sliding mode control. In *2019 8th International Conference on Power Systems (ICPS)* (pp. 1–6). IEEE. https://doi.org/10.1109/ICPS48983.2019.9067402

Peralta, D., Canizares, C., and Bhattacharya, K. (2021). Practical modeling of flywheel energy storage for primary frequency control in power grids. In *2021 IEEE Power and Energy Society General Meeting (PESGM)* (pp. 1–5). IEEE. https://doi.org/10.1109/PESGM.2018.8585844

Qu, H., and Ye, Z. (2023). Comparison of dynamic response characteristics of typical energy storage technologies for suppressing wind power fluctuation. *Sustainability, 15*(3), 2437. https://doi.org/10.3390/su15032437

Ray, P. K., and Mohanty, A. (2019). A robust firefly–swarm hybrid optimization for frequency control in wind/PV/FC based microgrid. *Applied Soft Computing, 85*, 105823. https://doi.org/10.1016/j.asoc.2019.105823

Rouniyar, A., and Karki, M. (2021, October). Energy management system for hybrid PV-Wind-Battery based standalone system. In *Proceedings of the 10th IOE Graduate Conference*. (pp. 131-138). https://conference.ioe.edu.np/ioegc10/papers/ioegc-10-018-10024.pdf

Saadat, H. (2002). *Power system analysis* (2nd ed.). McGraw-Hill.

Sahu, R. K., Gorripotu, T. S., and Panda, S. (2015). Automatic generation control of multi-area power systems with diverse energy sources using Teaching Learning Based Optimization algorithm. *Engineering Science and Technology, an International Journal, 19*(1), 113–134. http://dx.doi.org/10.1016/j.jestch.2015.07.011

Santhi, R. V., Sudha, K., and Devi, S. P. (2013). Robust load frequency control of multi-area interconnected system including SMES units using type-2 fuzzy controller. In *2022 IEEE International Conference on Fuzzy Systems (FUZZ-IEEE)* (Vol. 5, pp. 1–7). https://doi.org/10.1109/FUZZ-IEEE.2013.6622324

Sassi, A., Zaidi, N., Nasri, O., and Slama, J. B. H. (2017). Energy management of PV/wind/battery hybrid energy system based on batteries utilization optimization. In *2017 International Conference on Green Energy Conversion Systems (GECS)* (pp. 1–7). https://doi.org/10.1109/GECS.2017.8066133

Shareef, H., Ibrahim, A. A., and Mutlag, A. H. (2015). Lightning search algorithm. *Applied Soft Computing, 36*, 315–333. https://doi.org/10.1016/j.asoc.2015.07.028

Simpa, N. P., Solomon, N. N. O., Adenekan, N. O. A., and Obasi, N. S. C. (2024). The safety and environmental impacts of battery storage systems in renewable energy. *World Journal of Advanced Research and Reviews, 22*(2), 564–580. https://doi.org/10.30574/wjarr.2024.22.2.1398

Vishnuvardhan, V. Y., and Saravanan, B. (2023). Multimachine stability improvement with hybrid energy renewable system using a superconducting magnetic energy storage in power systems. *Journal of Energy Storage, 57*, 106255. https://doi.org/10.1016/j.est.2022.106255

Wang, S., Li, F., Zhang, G., and Yin, C. (2022a). Analysis of energy storage demand for peak shaving and frequency regulation of power systems with high penetration of renewable energy. *Energy*, *267*, 126586. https://doi.org/10.1016/j.energy.2022.126586

Wang, L., Cao, Q., Zhang, Z., Mirjalili, S., and Zhao, W. (2022b). Artificial rabbits optimization: A new bio-inspired meta-heuristic algorithm for solving engineering optimization problems. *Engineering Applications of Artificial Intelligence*, *114*, 105082. https://doi.org/10.1016/j.engappai.2022.105082

Worku, M. Y. (2022). Recent advances in energy storage systems for renewable source grid integration: A comprehensive review. *Sustainability*, *14*, 5985. https://doi.org/10.3390/su14105985

Xie, D., Wei, X., Ning, Y., Yang, S., and Zhou, Z. (2023). Power system restoration method with the flywheel energy storage support. In *2023 8th International Conference on Power and Renewable Energy (ICPRE)* (pp. 1028–1032).

https://doi.org/10.1109/ICPRE59655.2023.10353641

Yao, J., Yu, M., Gao, W., and Zeng, X. (2016). Frequency regulation control strategy for PMSG wind-power generation system with flywheel energy storage unit. *IET Renewable Power Generation*, *11*(8), 1082–1093. https://doi.org/10.1049/IET-RPG.2016.0047

Zhang, K., Mo, J., Liu, Z., Yin, W., Wu, F., and You, J. (2025). Life cycle environmental and economic impacts of various energy storage systems: Eco-efficiency analysis and potential for sustainable deployments. *Integrated Environmental Assessment and Management*. https://doi.org/10.1093/inteam/vjaf035